

# Precision electroforming of variable aspect ratio micro structures: simulation and validation

WCMNM  
2020

Honggang Zhang<sup>1</sup> Nan Zhang<sup>1\*\*</sup> Fengzhou Fang<sup>1,2\*</sup>

<sup>1</sup> Centre of Micro/Nano Manufacturing Technology (MNMT-Dublin), School of Mechanical & Materials Engineering, University College Dublin, Dublin 4, Ireland

<sup>2</sup> State Key Laboratory of Precision Measuring Technology and Instruments, Laboratory of Micro/Nano Manufacturing Technology (MNMT), Tianjin University, Tianjin 300072, China

\*Correspondence: [fengzhou.fang@ucd.ie](mailto:fengzhou.fang@ucd.ie)

\*\*Correspondence: [nan.zhang@ucd.ie](mailto:nan.zhang@ucd.ie)

## Abstract

Based on the designed star patterns having variable feature width of 20-320  $\mu\text{m}$  with the aspect ratio of 5-0.3125, this paper numerically and experimentally investigates mass transfer capability and electrodeposition process inside micro structures and their effects on microstructural replication accuracy. The results indicate that a diffusion-dominated mass transfer is dominated inside the micro structure with an aspect ratio of greater than 1, where maximum relative replication error of depth is up to  $\sim 21.5\%$  with an aspect ratio of 5. With the aspect ratio less than 1, the convection-dominated mass transfer can be significantly enhanced, where the minimum relative replication error of depth decreases to  $\sim 0.1\%$ . Additionally, the results also indicate that a low current density of  $18 \text{ A/m}^2$  should be used for defect-free electroforming of high-aspect-ratio micro structures.

**Keywords:** Micro electroforming; mass transfer; microstructural replication accuracy; diffusion layer thickness

## 1. Introduction

Micro electroforming of high-aspect-ratio micro structure is a challenging task, which is dependent on achievable feature size, replication accuracy, and defects-free filling [1, 2]. Mass transfer inside the narrow and tall micro structure during the electroforming process is problematic [3-6]. The ions diffusion is more difficult with the decrease of feature width, where the replication accuracy of micro feature can be influenced. Besides, super-conformal filling of micro structure is also difficult, accompanying the occurrence of defects inside the micro structure if improper process conditions are used [7, 8]. Such defects can be voids and seams that result in the pinch-off effect, affecting the performance and lifetime of the mould [6].

In this paper, a novel star pattern with a varying feature width of 20-320  $\mu\text{m}$ , corresponding to a variable aspect ratio of 5-0.3125, is proposed to promptly evaluate mass transfer capability and microstructural manufacturability using the electroforming process. The numerical models of mass transfer and electrodeposition are firstly established to reveal mass transfer and filling mechanisms inside the micro structures with various aspect ratios. The electroforming experiment is conducted to fabricate a nickel mould for validation. The microstructural replication accuracy is evaluated in terms of feature width, depth, aspect ratio, and filling profile. The interaction among mass transfer, electrodeposition profile, replication accuracy, and aspect ratio is elaborated.

## 2. Simulation and experimental methods

### 2.1. Pattern design

Figure 1 shows designed star patterns. Pattern 1 is sparsely divided into 78 parts, in which the feature width alters from 40 to 320  $\mu\text{m}$  and the depth is 100  $\mu\text{m}$ . Correspondingly, the aspect ratio changes from 2.5 to 0.3125. While pattern 2 consists of uniformly distributed circular sectors of 157 parts, where the feature width for each part changes from 20 to 160  $\mu\text{m}$  and the aspect ratio varies from 5 to 0.625 as the feature width increases. Additionally, concentric circular trench marks are designed among micro structures for quicker measurement of key dimensions.

### 2.2. Numerical models

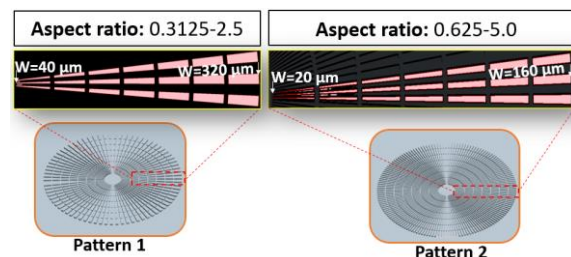


Fig. 1. Sketch of the star pattern design.

The lamina flow model is integrated into the dilute species transfer model for studying the mass transfer mechanism. The Nernst-Planck equation (1) is used to reveal the ion concentration. The tertiary current distribution model is used to compute the electrodeposition process with the level set interface to keep track of the deformation of the interface between the cathode surface and electrolyte. The Butler-Volmer equation (2) is used to express the local current density that is dependent on the potential and ion concentration.

$$\frac{\partial C_i}{\partial t} = \nabla \cdot \left( \underbrace{-C_i \mathbf{u}}_{\text{convection}} + \underbrace{D_i \nabla C_i}_{\text{diffusion}} + \underbrace{z_i \mu_i F C_i \nabla \Phi}_{\text{migration}} \right) + R \quad (1)$$

$$\begin{cases} i_{loc} = i_0 \left( \exp\left(\frac{1.5F\eta}{RT}\right) - \frac{C_{Cu^{2+}}}{C_{Cu^{2+},ref}} \exp\left(-\frac{0.5F\eta}{RT}\right) \right) \\ \eta = \phi_s - \phi_l - E_{eq} \end{cases} \quad (2)$$

where  $D_i$  is the diffusion coefficient of ion,  $\nabla$  is the Laplace operator,  $c_i$  is the ion concentration,  $u$  is the velocity field,  $z_i$  is the charge number,  $\mu_i$  is the mobility constant,  $F$  is the Faraday's constant,  $\phi$  is the electric potential.  $R$  is the production rate.  $i_{local}$ ,  $i_0$ ,  $T$  are the local current density, exchange current density, and temperature, respectively.  $\eta$ ,  $\phi_l$ ,  $\phi_s$ , and  $E_{eq}$  are the overpotential, electrolyte potential, cathode electrode potential, and equilibrium potential, respectively.

### 2.3. Experimental methods

Figure 2(a) shows a typical electroforming process method for fabricating a microstructured mould. A prepared silicon wafer with star patterns is used as a master template for replicating an invert nickel mould using the micro electroforming process. The micro electroforming process is performed using our customized precision micro electroforming machine, as shown in Figure 2(b). A wafer-scale microstructured nickel mould is shown in Figure 2(c). The related electroforming bath compositions and process parameters are shown in Table 1.

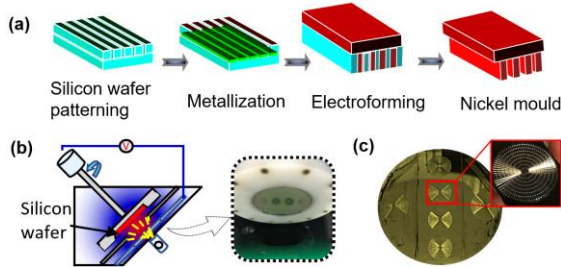


Fig. 2. (a) Schematic of the fabrication process of nickel mould; (b) electroforming setup; (c) electroformed nickel mould.

Table 1 Electrolyte compositions and electroforming process conditions.

Nickel sulfamate	400 g/L
Boric acid	35 g/L
Wetting agent	4 ml/L
Anode material	Nickel beads
Temperature	50°C
PH	4.0
Current density	18 A/m <sup>2</sup>
Cathode rotation speed	240 rpm

### 2.4. Measurement

A white light interferometer (NPFLEX, Bruker) is applied to measure microstructural width and depth along with the identifying marks in the patterns. Scanning Electron Microscope (SEM) (Topdesk 4000, Hitach) is used to observe replicated micro structures. An optical microscope (VHX-5000, Keyence) is used to inspect the cross-sectional morphology of micro structures.

## 3. Results and discussion

### 3.1. Simulation results and discussion on mass transfer

Figures 3(a-d) show the ion concentration distribution maps with different line widths of 20, 80, 160, and 320  $\mu\text{m}$ . The remarkable concentration gradient occurs at a high-aspect-ratio micro structure, especially for one with a width of 20  $\mu\text{m}$ . The leading ion transport is dominated by the diffusion process. With the feature width of 80  $\mu\text{m}$ , the convection boundary layer can move to the bottom of the micro structure and the concentration gradient is greatly reduced. The convection becomes the predominant mass transfer mechanism, and the diffusion layer thickness is shortened significantly. When the feature width is greater than 160  $\mu\text{m}$ , the convection completely controls mass transfer.

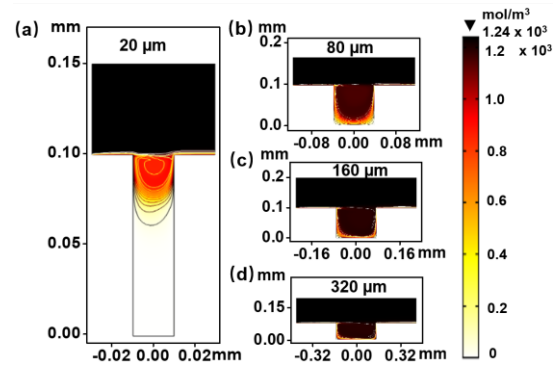


Fig. 3. The ions concentration distribution inside the micro structure with different feature widths.

The diffusion layer thickness is used to comprehensively evaluate the mass transfer capability inside the micro structure, as shown in Figure 4. As the feature width increases from 20 to 80  $\mu\text{m}$ , the diffusion layer thickness reduces from  $\sim 90$   $\mu\text{m}$  to  $\sim 60$   $\mu\text{m}$ , indicating a diffusion-dominated mass transfer within such a wide range. When the feature width is greater than 160  $\mu\text{m}$ , a dramatic reduction of diffusion layer thickness takes place and trends to be stable at  $\sim 10$   $\mu\text{m}$ . Thus, the microstructural feature width and aspect ratio are key factors affecting the electrolyte convection process.

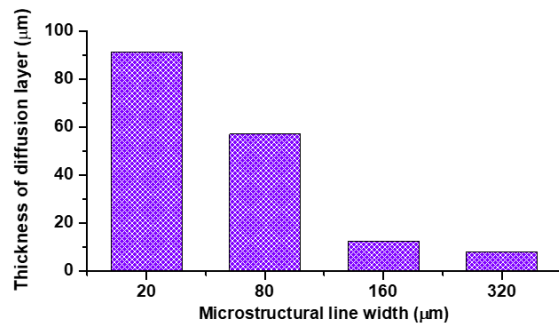


Fig. 4. The diffusion layer thickness inside the micro structure with different line widths.

### 3.2. Simulation results and discussion on microstructural electrodeposition

For the micro structure with a narrow feature width of 20  $\mu\text{m}$ , increased current causes different filling profiles with the evolution of defects varying from a void at a low current of 0.1 A to a seam at a current range of 0.2-1 A ((Figure 5(a))). For the micro structure with a feature width of 80  $\mu\text{m}$ , the filling quality is significantly improved with a small void (Figure 5(b)), compared to the cases of 20  $\mu\text{m}$ . When the feature width increases to 160  $\mu\text{m}$  (Figure 5(c)), the super-conformal filling profile is formed regardless of the applied current. Hence, it can be concluded that for the micro structure with a high aspect ratio of greater than 1, a low current of 0.1 A is required. While a large current can be applied in the micro structure with an aspect ratio less than 1.

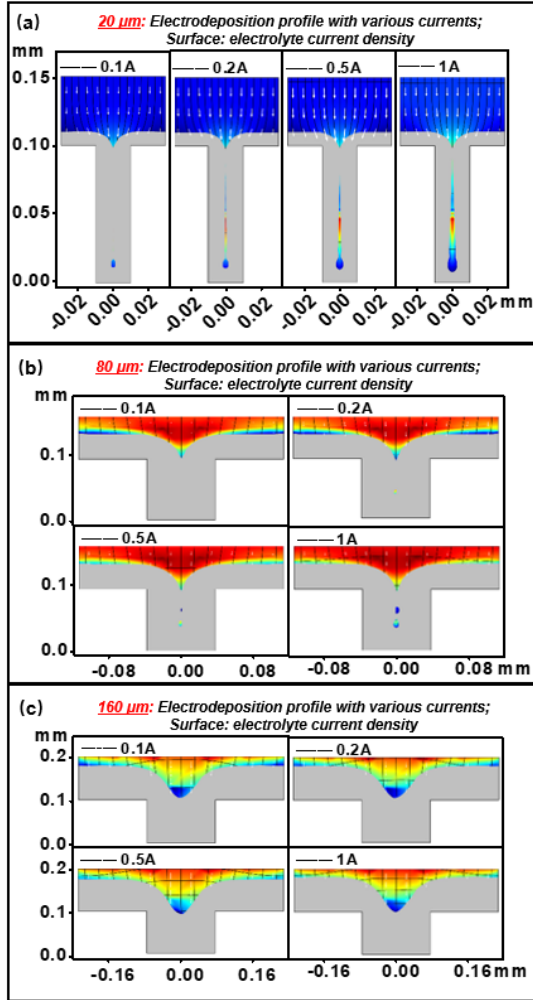


Fig. 5. Filling profile inside the micro structure with various feature widths under different currents: (a) 20  $\mu\text{m}$  wide under 0.1-1A; (b) 80  $\mu\text{m}$  wide under 0.1-1A; (c) 160  $\mu\text{m}$  wide under 0.1-1A.

### 3.3. Experimental results and discussion

Figure 6 shows the replicated line width, depth, aspect ratio, and their relative errors relevant to the designed width in the range of 20-320  $\mu\text{m}$ . It can be seen from Figure 6(a) that the maximum width relative error reaches  $\sim 9.5\%$ , where the designed line width is 20  $\mu\text{m}$ . When the designed feature width is greater than 40  $\mu\text{m}$ , the relative error can be controlled within 0-4%. Especially, it can be controlled within 2% for the

feature width greater than 160  $\mu\text{m}$ . For the electroformed depth in Figure 6(b), the replication accuracy is worse compared to the cases of replication in line width. The relative error presents a reducing trend as the designed feature width increases. When the designed line width is below 80  $\mu\text{m}$ , the relative error of depth is varying within 7%-21%. However, this relative error can be less than 5% for the designed line width greater than 100  $\mu\text{m}$ . The relative error of aspect ratio sharply decreases for the designed aspect ratio of 5-1.25. The maximum relative error reaches  $\sim 12.8\%$  at the aspect ratio of 5 (Figure 6(c)).

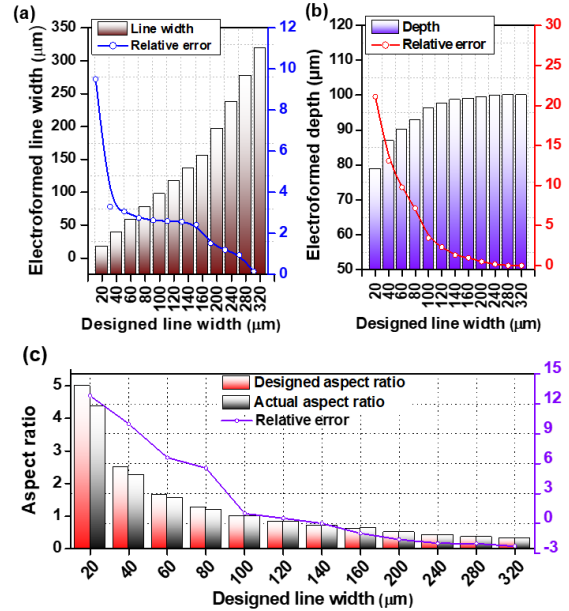


Fig. 6. The electroformed feature width, depth, aspect ratio, and their relative errors under the designed feature widths ranging from 20 to 320  $\mu\text{m}$ : (a) line width; (b) depth; (c) aspect ratio.

In addition, to elaborate the effect of mass transfer on the microstructural replication accuracy and to verify the effectiveness and feasibility of simulation results, the diffusion layer thickness is introduced to correlate the simulation and experiment for a straightforward comparison. Equation (3) can predict the related dependence among diffusion layer thickness, limiting current density, and electroformed thickness,

$$\begin{cases} h = \frac{itK}{1000\rho} \\ \delta = \frac{zFC D}{i(T-l)} \end{cases} \quad (3)$$

where  $\delta$  is the diffusion layer thickness,  $i$  is the limiting current density,  $z$ ,  $F$ ,  $C$ , and  $D$  are the participating charge, Faraday constant, the input molar concentration of nickel ions, and the electrolyte diffusion coefficient, respectively.  $T$  and  $l$  are the effective transportation number of ions and their transport number.  $h$  represents the electrodeposited relative thickness,  $t$ ,  $\rho$ , and  $K$  denote the electrodeposition time, the density of nickel, and the electrochemical equivalent of nickel, respectively.

It can be seen in Figure 7 that the reduction of diffusion layer thickness is obvious when the designed

line width is less than 80  $\mu\text{m}$ . When the designed line width is greater than 160  $\mu\text{m}$ , the diffusion layer thickness nearly tends to be stable. This variation tends to be well-matched with simulation results. Therefore, evident loss of replication accuracy of the micro structure with an aspect ratio greater than 1 (Figure 6) is due to the ion convection restricted in a narrow and tall micro structure with a thick diffusion layer. Nevertheless, the mass transfer can be enhanced for the micro structure with an aspect ratio less than 1, and thus the replication accuracy of the micro structure can be improved by reducing diffusion layer thickness.

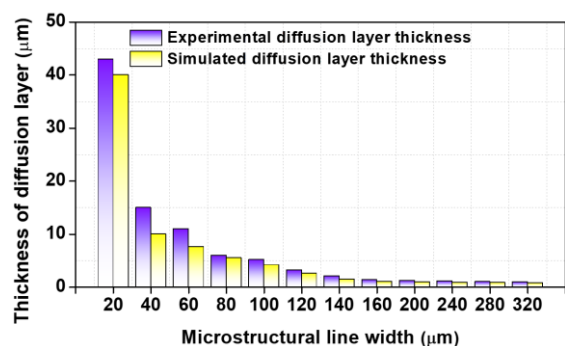


Fig. 7. The simulated and experimental diffusion layer thickness in the micro structure with various designed feature widths.

Figures 8(a-d) show the SEM images of the electroformed star patterns. The micro structures are well replicated, indicating a high-quality replication using electroforming. To observe the filling profile of micro structure, the cross-sectional morphology of the micro structure with various feature widths is investigated (Figure 8(e-h)). The defect-free filling is achieved no matter the aspect ratio is, and the steepness of the sidewall is satisfactory. This proves that the optimized current parameter from the simulation is reliable.

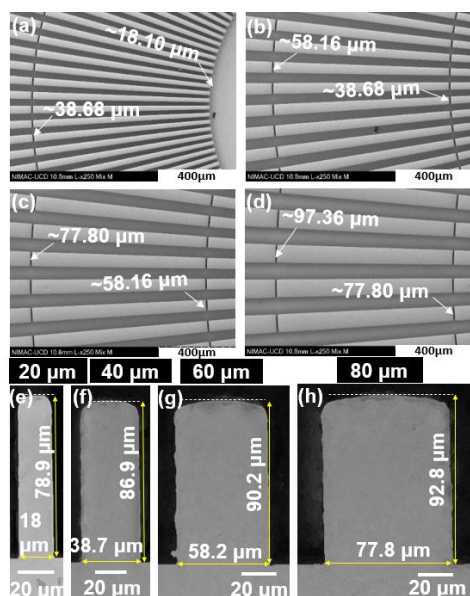


Fig. 8. (a-d) Surface morphologies of star patterns in different measurement marks; (e-h) cross-section morphologies of micro structures with various designed widths of 20, 40, 60, 80  $\mu\text{m}$ , respectively.

#### 4. Conclusions

Microstructural replication accuracy can be affected by mass transfer capabilities inside the micro structure with various feature widths and aspect ratios. When the aspect ratio is 5, the maximum width relative error is  $\sim 9.5\%$ . The maximum depth relative error comes to  $\sim 21\%$ , where the ion transportation is controlled by a diffusion-dominated mass transfer with a thick diffusion layer of  $\sim 40 \mu\text{m}$ . With the aspect ratio less than 1, the minimum width relative error is  $\sim 0.15\%$ ; and the minimum depth relative error is  $\sim 0.1\%$ , where the mass transfer is dominated by convection with a thin diffusion layer less than 1  $\mu\text{m}$ . Additionally, a low current density of 18  $\text{A}/\text{m}^2$  should be used for defect-free electroforming of a high-aspect-ratio micro structure.

#### Acknowledgments

The authors gratefully acknowledge the support from the Science Foundation Ireland (SFI) (No. 15/RP/B3208), the National Science Foundation of China (61675149), and the '111' project by the State Administration of Foreign Experts Affairs and the Ministry of Education of China (No. B07014).

#### References

- [1] Yang, H. et al. "High-aspect-ratio microstructural posts electroforming modeling and fabrication in LIGA process," *Microsystem technologies*, 2006; 12(3), pp. 187-192.
- [2] Hou, J. et al. "Characterization of manufacturability of microstructures for micro-injection moulding of micro devices using star patterns," *Journal of Micromechanics and Microengineering*, 2019; 30(2), p. 025001.
- [3] Zhao, M. et al. "Quantitative study of mass transfer in megasonic micro electroforming based on mass transfer coefficient: simulation and experimental validation," *Electrochimica Acta*, 2019; 297, pp. 328-333.
- [4] Tsai, T.-H. et al. "Two-dimensional simulations of ion concentration distribution in microstructural electroforming," *The International Journal of Advanced Manufacturing Technology*, 2011; 57(5-8), pp. 639-646.
- [5] Zhang, H. et al. "Investigation of mass transfer inside micro structures and its effect on replication accuracy in precision micro electroforming," *International Journal of Machine Tools and Manufacture*, 2021; p. 103717.
- [6] Zhang, H. et al. "Fabrication of high-performance nickel/graphene oxide composite coatings using ultrasonic-assisted electrodeposition," *Ultrasonics sonochemistry*, 2020; 62, p. 104858.
- [7] Liu, G. et al. "Fabricating HARMS by using megasonic assisted electroforming," *Microsystem technologies*, 2008; 14(9-11), pp. 1223-1226.
- [8] Zhang, H. et al. "Advances in precision micro/nano-electroforming: a state-of-the-art review," *Journal of Micromechanics and Microengineering*, 30(10), 2020; p. 103002.